Nanostructures

DOI: 10.1002/anie.200502722

Corrosion-Based Synthesis of Single-Crystal Pd Nanoboxes and Nanocages and Their Surface Plasmon Properties**

*Yujie Xiong, Benjamin Wiley, Jingyi Chen, Zhi-Yuan Li, Yadong Yin, and Younan Xia**

Corrosion can be broadly defined as "the damage to metal caused by reactions with its environment," and may take place in many different forms such as pitting, crevice etching, intergranular exchange, galvanic replacement, and dealloying.[1] Although corrosion is generally undesirable (automobile corrosion alone costs $16 billion annually!), it can be exploited as a versatile route to porous structures such as metal membranes.[2] While many solution-phase methods have been developed for synthesizing nanoparticles with well-controlled shapes,[3] it is still a great challenge to generate hollow nanostructures without involving exotic templates. We recently found that the galvanic replacement reaction between Ag templates and $HAuCl_4$ in an aqueous medium could lead to the formation of hollow nanostructures with controllable void size, wall porosity, and shell thickness.[4] More interestingly, the surface plasmon resonance (SPR) peaks of the resultant nanostructures could be continuously shifted from the blue (400 nm) to the near infrared (1200 nm) region by controlling the molar ratio of Ag to $HAuCl_4$ and thus the extent of replacement, alloying, and dealloying. Ideally, one would prefer a one-step synthesis that is able to tune the SPR properties of metal nanostructures without the requirement of templates made of a different metal. Here we demonstrate that corrosive etching of single-crystal Pd nanocubes could be used to transform them into nanoboxes and nanocages by controlling the reaction time.

As demonstrated in previous studies, Pd nanoparticles play an important role in hydrogen storage,[5] serve as the primary catalyst for the reduction of pollutants emitted from automobiles,[6] and facilitate organic reactions such as Suzuki, Heck, and Stille couplings.[7] Their performance could be tuned or improved for most of these applications by processing Pd nanostructures into hollow ones. For example, although solid Pd nanoparticles usually lose their catalytic activity after one round of Suzuki coupling reactions,[7a] hollow Pd spheres remained highly active for at least 24 rounds of reactions.[7b] While the SPR properties of Au and Ag have enabled many applications such as colorimetric sensing, nanoscale wave-guiding, and enhancement of electromagnetic fields and light transmission,[8] the SPR properties of Pd nanoparticles remain largely unexplored since Pd particles less than 10 nm in size give no resonance peak in the visible and near infrared regions.[9] Furthermore, the specific sensitivity of Pd towards hydrogen makes it especially interesting for fabricating SPR-based sensors for hydrogen gas.[10] We found by using discrete dipole approximation (DDA) calculations[11] that the resonant peak of Pd nanoshells with outer diameters of 48 nm could be tuned from 530 to 870 nm by tailoring their wall thickness from 6 to 3 nm. To demonstrate that Pd nanostructures with hollow interiors could indeed exhibit tunable SPR extinction peaks in the visible region we have synthesized single-crystal Pd nanoboxes and nanocages by a self-templating, corrosive pitting process.

The synthesis was conducted in a solution containing ethylene glycol, water, and poly(vinyl pyrrolidone) (PVP) with the addition of Na_2PdCl_4 as a precursor to Pd. The reaction can be divided into six distinctive stages based on both microscopic and spectroscopic observations. Reduction of $[PdCl_4]^{2-}$ to Pd atoms dominated up until $t = 18$ h (Figure 1a), with the Pd atoms nucleating and growing into nanocubes (with slightly truncated corners) with edge lengths of approximately 48 nm. Oxidative etching of the Pd nanocubes by O_2 (that is, corrosion) started to surpass the reduction process at $t = 20$ h. Small pits were observed in the surfaces of individual Pd nanocubes (Figure 1b), thus implying that the corrosion was initiated locally rather than uniformly over the entire surface of each cube. Over the next hour the interior of each cube became increasingly empty while the size of the hole in the surface started to shrink to form a box with relatively thick walls (Figure 1c). After another hour the void was further increased in size and each Pd cube evolved into a completely empty box with somewhat

[*] Dr. Y. Xiong, J. Chen, Prof. Y. Xia
Department of Chemistry
University of Washington
Seattle, WA 98195 (USA)
Fax: (+1) 206-685-8665
E-mail: xia@chem.washington.edu
B. Wiley
Department of Chemical Engineering
University of Washington
Seattle, WA 98195 (USA)
Prof. Z.-Y. Li
Laboratory of Optical Physics
Institute of Physics
Chinese Academy of Sciences
Beijing 100080 (P.R. China)
Dr. Y. Yin
The Molecular Foundry
Lawrence Berkeley National Laboratory
Berkeley, CA 94720 (USA)

[**] This work was supported in part by a grant from the NSF (DMR-0451788), a DARPA-DURINT subcontract from Harvard University, and a fellowship from the David and Lucile Packard Foundation. Y.X. is a Camille Dreyfus Teacher Scholar (2002). B.W. and J.C. thank the Center for Nanotechnology at the University of Washington for an IGERT (funded by the NSF, DGE-9987620) and a Nanotech fellowship, respectively. Z.-Y.L. was supported by the National Key Basic Research Special Foundation of China (Grant no. 2004CB719804). Y.Y. was supported by the Director, Office of Science, U.S. Department of Energy, under Contract DE-AC03-76SF00098. This work used the Nanotech User Facility (NTUF), a member of the National Nanotechnology Infrastructure Network (NNIN) funded by the NSF. We thank the Molecular Foundry at the Lawrence Berkeley National Laboratory for HRTEM analysis.

Supporting information for this article is available on the WWW under http://www.angewandte.org or from the author.

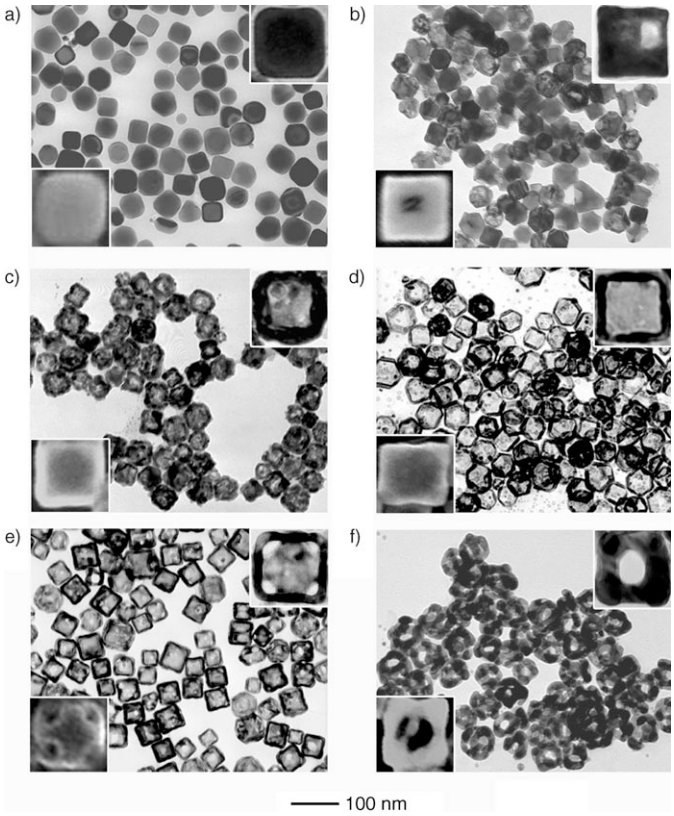

Figure 1. TEM images of the products at different reaction stages: a) $t = 18$ h; b) $t = 20$ h; c) $t = 21$ h; d) $t = 22$ h; e) $t = 24$ h; and f) $t = 28$ h. Note that the 100-nm bar applies to all images. The upper right and lower left insets show enlarged TEM and SEM images of an individual particle taken from each product, respectively.

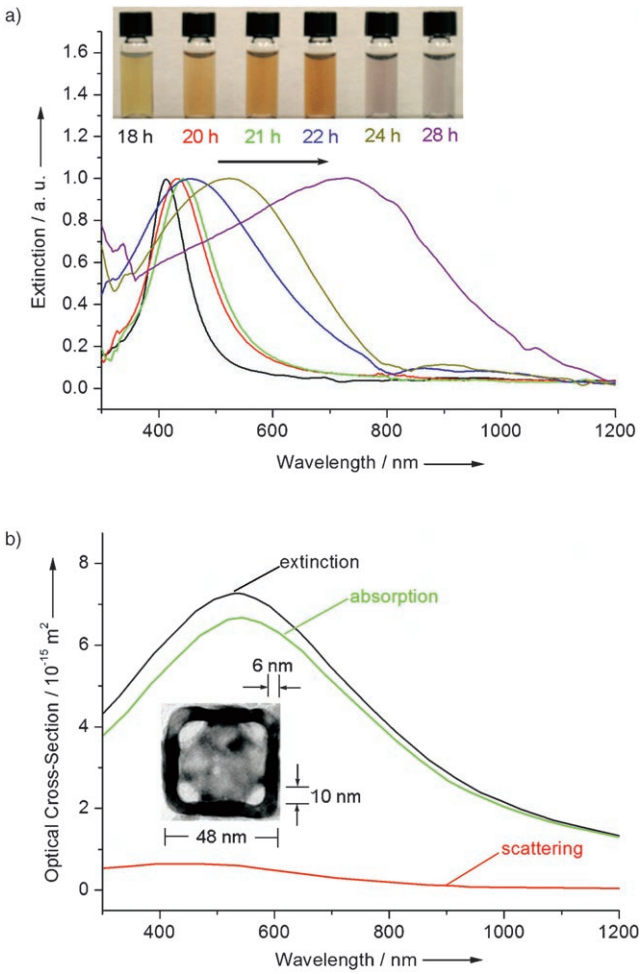

Figure 2. Surface plasmon properties of the Pd nanostructures shown in Figure 1: a) UV/Vis extinction spectra recorded from aqueous suspensions of the as-synthesized samples (see the inset, all spectra are normalized against the intensities of their strongest peaks); and b) DDA calculation of extinction, scattering, and absorption cross-sections of the Pd nanocage depicted in the inset.

truncated corners (Figure 1 d). Note that the hole in the surface had by now disappeared so that the nanobox was enclosed by a smooth, thin wall with a thickness of about 8 nm. Small holes appeared at the corners of each nanobox if the reaction was continued beyond this point. Holes of about 10 nm in diameter punctured each corner at $t = 24$ h (Figure 1 e), thus turning the nanobox into a cage. The Pd nanocage had an edge length of approximately 48 nm and was characterized by a uniform wall thickness of about 6 nm. It is worth noting that the outer diameter of the nanobox and nanocage exhibited no significant change relative to the initial Pd nanocube. The nanocage finally evolved into a ring (probably through additional etching and Ostwald ripening), thus causing the wall thickness to increase slightly from 6 to 10–20 nm (Figure 1 f).

The Pd nanostructures displayed distinctive colors since SPR is strongly dependent on wall thickness. As shown by the inset in Figure 2 a, the aqueous suspensions changed from yellow to orange to purple as the solid Pd nanocubes were transformed into hollow boxes and then porous cages. Figure 2 a shows the UV/Vis extinction spectra recorded from the six aqueous suspensions. The Pd nanocubes exhibited an SPR peak at 410 nm, which was consistent with the results of DDA calculations (see the Supporting Information).[11] The SPR peak was red-shifted to 430 nm as holes appeared in their surfaces. The formation of hollow structures with thick walls (and relatively rough inner surfaces) resulted in the sample exhibiting an SPR peak at 443 nm. The extinction peak was further shifted to 452 nm as the wall of the nanoboxes was thinned to 8 nm. Once the product had evolved into nanocages with an edge length of 48 nm and a wall thickness of 6 nm, the SPR peak was shifted to 520 nm, which matched the calculated spectra (Figure 2 b). The extinction (C_{ext}), absorption (C_{abs}), and scattering (C_{sca}) cross-sections are related by the following equation: $C_{ext} = C_{abs} + C_{sca}$.

Figure 3 a and b show typical SEM and TEM images of the Pd nanoboxes at relatively low magnifications which indicate that over 95% of the hollow structures inherited the truncated, cubic shape of the initial cubes. The fringes in the HRTEM images (Figure 3 c and d) showed a period of 2.0 Å, which was consistent with the {200} lattice spacing of face-centered-cubic Pd. These images also displayed well-resolved, continuous fringes with the same orientation, thus implying that the Pd nanobox, like the starting Pd nanocube, was a piece of single crystal. The inset of Figure 3 c shows a

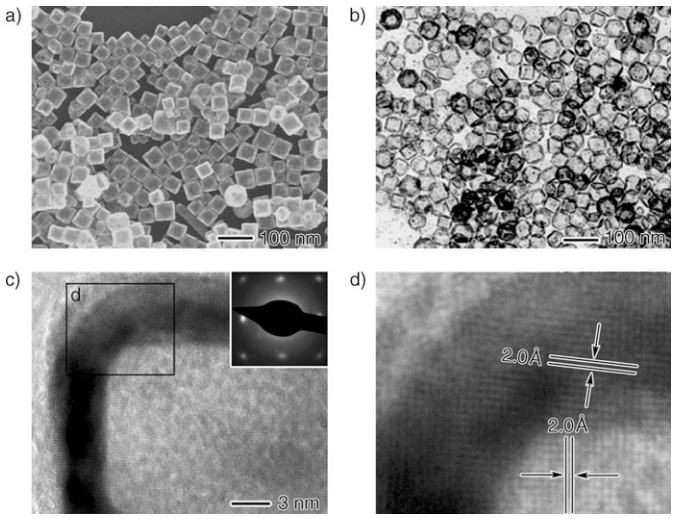

Figure 3. Electron microscopy characterization of the Pd nanoboxes obtained at $t = 22$ h: a) SEM image; b) TEM image; and c, d) high-resolution TEM images. The inset of (c) shows an electron diffraction pattern taken from the side surface of an individual Pd nanobox.

nanoprobe electron diffraction (ED) pattern obtained by aligning the beam perpendicular to one of the side faces of a cubic box. The spots could be indexed to the {200} diffraction of face-centered-cubic Pd. This diffraction pattern also suggests that the Pd nanobox was a single crystal with its symmetry similar to that of the initial Pd nanocube, which was enclosed by {100} facets. Both powder XRD and microprobe ED patterns (see the Supporting Information) further confirms the high phase purity and crystallinity of the Pd nanoboxes.

To analyze the corrosive etching process that transformed Pd nanocubes into nanocages we recorded UV/Vis spectra of the solution at different stages of the reaction (see the Supporting Information, the Pd nanoparticles were removed by centrifugation before the spectra were taken). The extinction peak at 242 nm (see the Supporting Information) corresponds to $[PdCl_4]^{2-}$ while that at 278 nm can be attributed to water-substituted $[PdCl_4]^{2-}$ ($[PdCl_{4-n}(H_2O)_n]^{(2-n)-}$) species.[12] The peak at 242 nm disappeared quickly when $[PdCl_4]^{2-}$ was reduced by ethylene glycol to generate Pd atoms and then nanocubes (see the Supporting Information). The concentration of water-substituted $[PdCl_4]^{2-}$ steadily increased as the nanocubes were etched by corrosive pitting. Similar to the corrosion of bulk metals,[13] O_2, Cl^- ions, and H_2O are all instrumental for the initiation of pitting on the surfaces of Pd nanocubes. As documented in the literature, corrosion most commonly occurs when the O_2 in air is dissolved in a thin film of water on the surface of a metal, thereby picking up electrons from the cathode to form hydroxide ions that then migrate towards the anode.[1] If the anode and cathode are located at different sites on the metal surface because of differences in the local environment (for example, surface heterogeneity and/or concentrations of ions), either pitting or crevice corrosion will take place.[1] Like the corrosion of bulk metals, adsorption of chloride ions can greatly increase the rate of surface diffusion and therefore expedite the pitting process.[13] On the other hand, the presence of a small amount of water can enhance the solubility of O_2 and profoundly increase the corrosion rate.[1] In addition to the augmentation by O_2, Cl^- ions, and H_2O, the amount of PVP was also found to be critical to the formation of hollow Pd nanostructures through a corrosion process. A large amount of PVP (with the ratio of PVP to Pd being 15:1) could ensure that the surface of each Pd nanocube was effectively covered by this polymer. In addition, the surface of each Pd nanocube is likely covered by a thin layer of palladium oxide.[13a] Both of these factors could make the surface of a Pd nanocube less reactive than the freshly exposed interior once the pitting process has started.[13b]

Figure 4 summarizes all the major steps involved in the corrosive etching process. Compared with the system without water (which produced Pd particles ca. 8 nm in size),[12b] the presence of water significantly accelerated the oxidative etching of Pd, and thus reduced the number of seeds formed in the nucleation step. As we have recently demonstrated in a case where Fe^{III} ions were added as the oxidative etchant,[14] a decrease in the number of seeds resulted in formation of Pd nanocubes with larger sizes when the concentration of the Pd precursor was maintained. As in the corrosion of bulk metals, the presence of water also facilitated the pitting process. Once a pit was formed at a specific site on the surface of a Pd cube (step a), further corrosion would occur preferentially inside

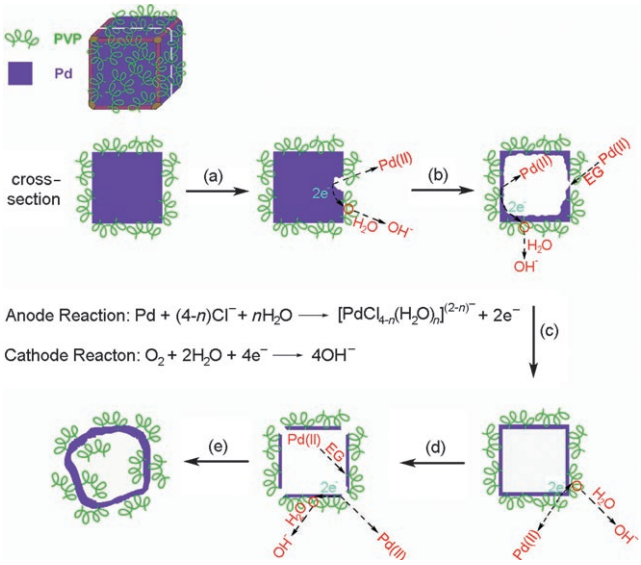

Figure 4. Schematic illustration summarizing all the major morphological changes involved in the synthesis of Pd nanoboxes and nanocages by corrosive etching: a) Pitting at a specific site on the surface of a nanocube where the O_2 dissolved in the solvent received electrons from the cathode and generated hydroxide ions that migrated towards the anode; b) formation of hollow structures after further etching of the interior of the nanocube, and the concentration of water-substituted $[PdCl_4]^{2-}$ increased; c) formation of a completely enclosed Pd nanobox by reducing the water-substituted $[PdCl_4]^{2-}$ species to form Pd atoms at the edge of each hole; d) formation of nanocages by dissolving Pd from the corners of the nanobox; and e) reconstruction of the nanocage by relocating all the holes from the corners to side faces and thickening of the wall as a result of additional reduction of the water-substituted $[PdCl_4]^{2-}$ species.

the pit, thus leading to formation of a hollow nanostructure (step b). As etching was continued, the concentration of water-substituted $[PdCl_4]^{2-}$ sufficiently increased to allow the reduction by ethylene glycol to take place at the edge of a hole, thus causing it to gradually shrink in size. Since the reduction of water-substituted $[PdCl_4]^{2-}$ by ethylene glycol was minimal, most of these ionic species were retained in the solution rather than being reduced and deposited onto the outer surface of the Pd nanoboxes. This argument is supported by the UV/Vis spectra (see the Supporting Information), and it is for this reason why the outer dimensions of the Pd nanocubes, nanoboxes, and nanocages were essentially the same. It is the combination of continuous etching of the Pd nanocube from the interior and some reduction of the Pd^{II} species at the edge of the hole that resulted in the formation of Pd nanobox by $t = 22$ h (step c). It is worth pointing out that such a self-templating and self-etching process has also been observed in the solution-phase synthesis of ZnO microtubes.[15] The Pd nanoboxes were as unstable as the nanocubes when exposed to the corrosive environment. Under the illumination of light, the electric field intensity should concentrate at the corners, thus increasing the surface charge at these sites.[16] As a result, corrosive etching of the Pd nanoboxes preferentially occurred at the corners, thus leading to the formation of Pd nanocages with all eight corners being truncated (step d). This is different from the synthesis performed in the dark (see the Supporting Information). Further corrosion caused these holes to increase in dimension until the Pd nanocages evolved into rings. At the same time, continuous reduction of the water-substituted $[PdCl_4]^{2-}$ species occurred on the exterior surface of the nanocages, which led to the formation of nanorings (step e). This course of materials transfer resembles the conventional "Ostward ripening" process. Overall, the void size, shell thickness, and wall porosity of Pd hollow nanostructures were determined by the net difference between two opposite reactions: the reduction of the Pd^{II} precursor to form Pd^0 atoms, and the oxidation of Pd (both atoms and nanostructures) into Pd^{II} species.

In summary, metal corrosion is a familiar and common natural phenomenon that, while normally viewed as a detrimental process that destroys the usefulness of tools and machines, can also serve as a simple, elegant, and powerful method for the fabrication of hollow nanostructures with controllable optical properties. More specifically, corrosive pitting and etching could be combined to transform single-crystal Pd nanocubes into nanoboxes and nanocages in a one-pot synthesis without the involvement of exotic templates. The SPR peaks of Pd nanostructures could be tuned from 410 to 520 nm by empting their interiors. Our DDA calculations indicated that the SPR peak of the Pd nanocages with edge lengths of 48 nm could be further red-shifted to 870 nm by decreasing their wall thickness to 3 nm.

Experimental Section

In a typical synthesis, ethylene glycol (5 mL, J. T. Baker) was placed in a 3-neck flask (equipped with a reflux condenser and a teflon-coated magnetic stirring bar) and heated in air at 100 °C for 1 h. Meanwhile, palladium(II) sodium chloride (0.0486 g, Na_2PdCl_4, Aldrich) and poly(vinyl pyrrolidone) (0.2747 g, PVP, M.W. = 55000, Aldrich) were dissolved at room temperature in ethylene glycol (3 mL) and water (3 mL), respectively. These two solutions (with the molar ratio between Pd and the repeating unit of PVP being 1:15) were then injected simultaneously into the flask with a syringe pump at a rate of 45 mL h^{-1}. Heating of the reaction at 100 °C was continued in air for 28 h. A set of samples were taken over the course of a synthesis with a glass pipette. To minimize temperature perturbation during sampling, the glass pipette was held just above the solution and preheated for 30 s before immersion. For the argon-protected synthesis, all other experimental parameters were kept the same except for the continuous bubbling of argon. The samples were washed with acetone and then with ethanol several times before they were centrifuged at a rate of 6000 rpm for 10 min to remove most of the ethylene glycol and excess PVP. The samples were characterized by transmission electron microscopy (TEM), high-resolution TEM, scanning electron microscopy (SEM), electron diffraction (ED), and powder X-ray diffraction (PXRD).

TEM images and microprobe ED patterns were recorded on a Phillips 420 transmission electron microscope operated at 120 kV. HRTEM images and nanoprobe ED patterns were taken on a Jeol 2010 LaB6 high-resolution transmission electron microscope operated at 200 kV. PXRD patterns were recorded on a Philips 1820 diffractometer equipped with a $Cu_{K\alpha}$ radiation source ($\lambda = 1.54180$ Å). SEM images were taken on a FEI field-emission scanning electron microscope (Sirion XL) operated at an accelerating voltage of 20 kV. UV/Vis spectra were obtained using a Hewlett–Packard 8452A diode array spectrophotometer.

The calculation used in the article is based on the DDA method.[11] DDA is a computational method developed for studying both the scattering and absorption of electromagnetic radiation by particles with sizes on the order of or smaller than the wavelength of incident light. In the calculation, the particle is divided into an array of N polarizable point dipoles, each of which is characterized by a polarizability of $\boldsymbol{\alpha}_i$. When the system is excited by a monochromatic incident plane wave $\boldsymbol{E}_{inc}$, each dipole of the system will be subjected to an electric field that can be split in two contributions: 1) the incident radiation field $\boldsymbol{E}_{i,inc}$ and 2) the field radiated by all of the other induced dipoles $\boldsymbol{E}_{i,dip}$. The sum of both fields is the so-called local field at each dipole ($\boldsymbol{E}_{i,loc} = \boldsymbol{E}_{i,inc} + \boldsymbol{E}_{i,dip}$). Each dipole can be expressed as an oscillating polarization with the dipole moment being $\boldsymbol{P}_i = \boldsymbol{\alpha}_i \boldsymbol{E}_{i,loc}$. Both absorption and scattering cross-sections (C_{abs} and C_{sca}) can be obtained directly from $\boldsymbol{P}_i$. The refractive index of bulk Pd was used in all calculations reported in this article, and the nanoparticle was assumed to be surrounded by and filled with water (when it became porous).

Received: August 3, 2005
Published online: November 22, 2005

Keywords: corrosion · nanostructures · palladium · scanning probe microscopy · surface plasmon resonance

[1] S. A. Bradford, *Corrosion Control*, 2nd ed., CASTI Publishing, Edmonton, Canada, **2001**, pp. 1–51.
[2] Y. Ding, J. Erlebacher, *J. Am. Chem. Soc.* **2003**, *125*, 7772–7773.
[3] a) F. Kim, S. Connor, H. Song, T. Kuykendall, P. Yang, *Angew. Chem.* **2004**, *116*, 3759–3763; *Angew. Chem. Int. Ed.* **2004**, *43*, 3673–3677; b) V. F. Puntes, K. M. Krishnan, A. P. Alivisatos, *Science* **2001**, *291*, 2115–2117; c) L. A. Gugliotti, D. L. Feldheim, B. E. Eaton, *Science* **2004**, *304*, 850–852; d) X. Teng, H. Yang, *Nano Lett.* **2005**, *5*, 885–891.
[4] a) Y. Sun, Y. Xia, *Science* **2002**, *298*, 2176–2179; b) Y. Sun, Y. Xia, *J. Am. Chem. Soc.* **2004**, *126*, 3892–3901; c) B. Wiley, Y.

Sun, J. Chen, H. Cang, Z.-Y. Li, X. Li, Y. Xia, *MRS Bull.* **2005**, *30*, 356 – 361.
[5] Y. Sun, Z. Tao, J. Chen, T. Herricks, Y. Xia, *J. Am. Chem. Soc.* **2004**, *126*, 5940 – 5941.
[6] Y. Nishihata, J. Mizuki, T. Akao, H. Tanaka, M. Uenishi, M. Kimura, T. Okamoto, N. Hamada, *Nature* **2002**, *418*, 164 – 167.
[7] a) Y. Li, X. M. Hong, D. M. Collard, M. A. El-Sayed, *Org. Lett.* **2000**, *2*, 2385 – 2388; b) S.-W. Kim, M. Kim, W. Y. Lee, T. Hyeon, *J. Am. Chem. Soc.* **2002**, *124*, 7642 – 7643; c) M. T. Reetz, E. Westermann, *Angew. Chem.* **2000**, *112*, 170 – 173; *Angew. Chem. Int. Ed.* **2000**, *39*, 165 – 168; d) S. U. Son, Y. Jang, J. Park, H. B. Na, H. M. Park, H. J. Yun, J. Lee, T. Hyeon, *J. Am. Chem. Soc.* **2004**, *126*, 5026 – 5627.
[8] Y. Xia, N. J. Halas, *MRS Bull.* **2005**, *30*, 338 – 343.
[9] J. A. Creighton, D. G. Eadon, *J. Chem. Soc. Faraday Trans.* **1991**, *87*, 3881 – 3891.
[10] P. Tobiška, O. Hugon, A. Trouillet, H. Gagnaire, *Sens. Actuators B* **2001**, *74*, 168 – 172.
[11] a) W. H. Yang, G. C. Schatz, R. P. Van Duyne, *J. Chem. Phys.* **1995**, *103*, 869 – 875; b) K. L. Kelly, E. Coronado, L. L. Zhao, G. C. Schatz, *J. Phys. Chem. B* **2003**, *107*, 668 – 677; c) I. O. Sosa, C. Noguez, R. G. Barrera, *J. Phys. Chem. B* **2003**, *107*, 6269 – 6275.
[12] a) B. Veisz, Z. Király, *Langmuir* **2003**, *19*, 4817 – 4824; b) Y. Xiong, J. Chen, B. Wiley, Y. Xia, S. Aloni, Y. Yin, *J. Am. Chem. Soc.* **2005**, *127*, 7332 – 7333.
[13] a) R. C. Newman, K. Sieradzki, *Science* **1994**, *263*, 1708 – 1709; b) J. C. Scully, *The Fundamentals of Corrosion*, 3rd ed., Pergamon, Oxford, **1990**, pp. 1 – 57.
[14] Y. Xiong, J. Chen, B. Wiley, Y. Xia, Y. Yin, Z.-Y. Li, *Nano Lett.* **2005**, *5*, 1237 – 1242.
[15] L. Vayssieres, K. Keis, A. Hagfeldt, S. E. Lindquist, *Chem. Mater.* **2001**, *13*, 4395 – 4398.
[16] a) J. P. Kottmann, O. J. F. Martin, D. R. Smith, S. Schultz, *Phys. Rev. B* **2001**, *64*, 235402(1 – 10); b) A. J. Haes, C. L. Haynes, A. D. McFarland, G. C. Schatz, R. P. Van Duyne, S. Zhou, *MRS Bull.* **2005**, *30*, 368 – 375.

